PERGAMON

International Journal of Heat and Mass Transfer 44 (2001) 1899–1911

International Journal of HEAT and MASS TRANSFER

www.elsevier.com/locate/ijhmt

Model reduction for the resolution of multidimensional inverse heat conduction problems

E. Videcoq, D. Petit *

Laboratoire d'Études Thermiques – UMR, CNRS 6608, ENSMA, BP 109, 86960 Futuroscope Cedex, France

Received 28 July 1999; received in revised form 10 July 2000

Abstract

For large linear heat conduction systems, it is proposed here to solve an inverse heat conduction problem (IHCP) that consists in the identification of several time-varying thermal solicitations from simulations of measured temperatures. For this inversion, instead of using a detailed model of large size, this one is first transformed into a reduced model. The latter is built with identified dominant eigenmodes of the system leading to a reduced state representation that links the inputs (unknown solicitations) to the outputs (simulated temperatures). The procedure is sequential and uses future time steps. At first, a numerical 2D IHCP is provided: two time-varying heat flux densities are estimated from various positions of two sensors. A specific study on static and dynamic sensitivities is made. An example of a 3D IHCP is also given. The method is particularly interesting in this last case where, at each time step, the resolution of a system of order 9 (the reduced model) takes the place of a system of order 1331 (the detailed model).

1. Introduction

Among the several types of inverse heat conduction problems (IHCP), we are interested here in the identification of unknown boundary conditions varying in time from the knowledge of temperature evolutions at some points of the domain. Numerous works concerning this mathematically ill-posed problem have already been carried out. In a non-exhaustive manner, we shall underline Beck's contribution [1–3,6] which takes into account the lagging and damping effects due to the diffusion process by using a sequential method associated to a function specification procedure. This technique acts as an efficient regularization procedure, as it will be shown in this paper. Other kinds of regularization techniques are also very often used in IHCPs as, for example, Tikhonov's method [2,3,6] and the iterative regularization [4,5]. According to the geometry, we can point out:

- in 1D problems: the space-marching scheme [7], a recursive least squares algorithm [8], the use of Kalman's smoothing technique [9],
- in 2D: another Kalman's approach [10], the combination of Tikhonov's regularization with boundary element method (BEM) [11–13], and with the function specification method in a non-linear case [6],
- in 3D: a theoretical paper using the adjoint equation approach coupled to the conjugated gradient is proposed [14]. For a stationary case, the identification of a field of heat transfer coefficients is given [15].

All these IHCPs involve temperature measurements (real or simulated) associated with a mathematical representation. Except for very special cases where the model is analytical, as soon as the geometry, or the boundary conditions become complicated, it is then necessary to use a model leaning on a spatial discretization of the domain (finite elements, control volume method, boundary element method, ...). These methods can lead to a system of N differential equations as follows:

$$\boldsymbol{C}_a\dot{T}(t) = \boldsymbol{K}T(t) + \boldsymbol{\Psi}(t), \tag{1}$$

where t is the time, T (dim N) the vector of the N temperatures at the grid nodes and $\dot{T}$ is its derivative with

* Corresponding author. Tel.: +33-5-4949-8113; fax: +33-5-4949-8101.

E-mail addresses: videcoq@let.ensma.fr (E. Videcoq), petit@let.ensma.fr (D. Petit).

0017-9310/01/$ - see front matter
PII: S0017-9310(00)00239-8

Nomenclature

$\boldsymbol{A}(N,N)$	state space matrix for DM
$\boldsymbol{B}(N,p)$	command matrix for DM
$\boldsymbol{C}(q,N)$	output matrix
$\mathbf{C}(q^*(nf+1),np)$	macro matrix
$\boldsymbol{f}(m,m)$	diagonal matrix relative to current ERM [s^{-1}]
$\mathbf{F}(N,N)$ [or (n,n)]	diagonal matrix of eigenvalues for DM [or RM] [s^{-1}]
$g(m)$	vector applying $\dot{u}$
$\boldsymbol{G}(N,p)$ [or (n,p)]	input (or command) matrix for DM [or RM]
$\boldsymbol{h}(q,m)$	output matrix relative to current ERM
$\boldsymbol{H}(q,N)$ [or (q,n)]	output (or observation) matrix for DM [or RM]
k	thermal conductivity [$W\,m^{-1}\,°C^{-1}$]
m	order of current ERM
n	order of RM ($n=\sum m$)
N	order of DM
nf	number of future times for specification function
nt	number of time steps for simulation
p	dimension of input vector
q	dimension of output vector
$s(q)$	static vector relative to current ERM
$\boldsymbol{S}(q,p)$	static matrix, static sensitivity matrix
$S_{i,j}$	static sensitivity of sensor $n°i$ relatively to input $n°j$
$\boldsymbol{S}_{\mathrm{d}}(q,p)$	dynamic sensitivity matrix
$S_{di,j}$	dynamic sensitivity of sensor $n°i$ relatively to input $n°j$
$T,\dot{T}(N)$	temperature vector, its derivative
$u,\dot{u}$	current component of U, its derivative
$U,\dot{U}(p)$	input vector, its derivative
$x,\dot{x}(m)$	ERM state vector, its derivative
$X,\dot{X}(N)$ [or (n)]	state vector in modal form, its derivative for DM [or RM]
$y(q)$	ERM output vector
$Y(q)$	output vector for DM [or RM]
$Y_m(q)$	output vector of simulated measurements
$\mathbf{Y}(q^*(nf+1))$	macro output vector

Abbreviations

DM	detailed model
ERM	elementary reduced model
FTS	future time step
RM	reduced mode

Greek symbols

Δt	time step [s]
ρ	density [$kg\,m^{-3}$]
σ	standard deviation of the measured temperatures [°C]
σ_U	root mean square for U [$W\,m^{-2}$]
σ_Y	root mean square for Y [°C]
τ	time constant [s]
φ	heat flux density [$W\,m^{-2}$]
$\psi(N)$	vector of thermal excitations
ω	random variable

Superscripts

$\hat{}$	estimated value
$^{\mathrm{T}}$	transposition sign

respect to time. The matrices $\boldsymbol{C}_a$ (heat capacity) and $\boldsymbol{K}$ (thermal conductance) are constant for a linear problem. This physical model will be called a detailed model (DM). If such a DM is satisfactory in the direct simulation (computation of the temperature field, when knowing the heat sources and boundary conditions included in Ψ), it becomes much harder for IHCP: the number N of the nodes of the discretization is usually large compared to the number of sensors q ($q \ll N$). These sensor temperatures represent only a part of vector T written as

$$Y(t) = \boldsymbol{C}T(t), \tag{2}$$

where $\boldsymbol{C}$ (dim. q,N) is a selecting matrix.

So, instead of using such a DM to invert, i.e., to identify the heat solicitations included in Ψ from the knowledge of $Y(t)$, it is proposed here to use a reduced model (RM) which is low dimensioned and which connects the inputs to the observed outputs through a small-dimensioned state representation based on dominant eigenmodes of the system: the assumptions of linearity and invariance are then necessary [16].

Coming from automatics [17,18], reduction methods have been applied and developed in thermal sciences [19,20]. Instead of using Eqs. (1) and (2), the state-space representation is used for model reduction. It is written as:

$$\dot{T}(t) = \boldsymbol{A}T(t) + \boldsymbol{B}U(t), \tag{3a}$$

$$Y(t) = \boldsymbol{C}T(t), \tag{3b}$$

where T (dim. N) is the state vector, $\boldsymbol{A}$, $\boldsymbol{B}$, $\boldsymbol{C}$ are respectively the state, input and output matrices such as:

$$\boldsymbol{A} = \boldsymbol{C}_a^{-1}\mathbf{K}, \tag{4}$$

$$\boldsymbol{C}_a^{-1}\Psi(t) = \boldsymbol{B}U(t). \tag{5}$$

For model reduction, the aim is then to compute another state-space representation with a very low-dimensional state vector $X(t)$ compared to the initial one $T(t)$ and that gives a very good approximation of the output vector $Y(t)$. The originality of the present work will consist in the use of such a model to invert.

Many of these reduction techniques lean on a selection of eigenmodes of the state matrix $\boldsymbol{A}$ of Eq. (3a) [17–20]. Whereas these methods require a matrix diagonalization – that can be heavy to handle if the system is large – as far as we are concerned, we have developed a reduction method leaning on the identification of a few representative eigenvalues [21–23].

This paper includes several parts. At first, our specific reduction method is recalled. The inverse method is then developed through the time discretization and the use of future time steps as a regularization procedure. An application on a 2D diffusive system is then shown. A 3D extension completes the study.

2. Reduction method

Our reduction method (RM), using another state-space representation than Eqs. (3a) and (3b) is recalled here. It takes into account the derivative of the input vector with respect to time.

2.1. Transformation of the state-space equations of DM

Consider a constant input vector $U_{\text{cst.}}$ From Eq. (3a), the corresponding state vector T_{cst} is then

$$T_{\text{cst}} = -\boldsymbol{A}^{-1}\boldsymbol{B}U_{\text{cst}}. \tag{6}$$

This would suggest the introduction of a new state vector T' with the following change of variable:

$$T(t) = T'(t) - \boldsymbol{A}^{-1}\boldsymbol{B}U(t). \tag{7}$$

Eqs. (3a) and (3b) then become

$$\dot{T}'(t) = \boldsymbol{A}T'(t) + \boldsymbol{A}^{-1}\boldsymbol{B}\dot{U}(t), \tag{8a}$$

$$Y(t) = \boldsymbol{C}T'(t) + \mathbf{S}U(t) \tag{8b}$$

with $\dot{U}(t)$ the derivative with respect to time of the input vector U and $\boldsymbol{S}$ is called the static matrix and is defined by

$$\boldsymbol{S} = -\boldsymbol{C}\boldsymbol{A}^{-1}\boldsymbol{B}. \tag{9}$$

Now, if we use the Jordan transformation to obtain a modal representation then Eqs. (8a) and (8b) become:

$$\dot{X}(t) = \boldsymbol{F}X(t) + \boldsymbol{G}\dot{U}(t), \tag{10a}$$

$$Y(t) = \boldsymbol{H}X(t) + \boldsymbol{S}U(t), \tag{10b}$$

where X is the new state vector in the modal base, $\boldsymbol{F}$ the diagonal matrix of eigenvalues, $\boldsymbol{G}$ and $\boldsymbol{H}$ the new input and output matrices i.e.:

$$X = \boldsymbol{M}^{-1}T', \quad \boldsymbol{G} = \boldsymbol{M}^{-1}\boldsymbol{A}^{-1}\boldsymbol{B}, \quad \boldsymbol{H} = \boldsymbol{C}\boldsymbol{M},$$
$$\boldsymbol{F} = \boldsymbol{M}^{-1}\boldsymbol{A}\boldsymbol{M} = \operatorname{diag}(F_i), \tag{11}$$

and $\boldsymbol{M}$ is the matrix constituted by eigenvectors (modal matrix).

This formulation allows the decoupling of state variables and consequently makes numerical integration easier. This formulation also gives information about the time constants τ_i of the system since eigenvalues f_i are

$$\text{real part of } (F_i) = -1/\tau_i. \tag{12}$$

In the case of diffusive heat transfer, we are interested in all the eigenvalues are real negative.

Remark. Note that these changes of variable are made on a detailed state-space model of order N on Eqs. (8a) and (8b). These developments are only made to introduce the structure of Eqs. (10a) and (10b) that will be used for the reduced model of order n. In the following paragraphs, we will not use this representation for the detailed model: Eqs. (3a) and (3b) will be kept.

2.2. Structure of reduced model

The important assumption here is that Eqs. (10a) and (10b) will be considered here as a form for our RM that will be therefore written as:

$$\dot{X}_{\text{R}}(t) = \boldsymbol{F}_{\text{R}}X_{\text{R}}(t) + \boldsymbol{G}_{\text{R}}\dot{U}(t), \tag{13a}$$

$$\hat{Y} = \boldsymbol{H}_{\text{R}}X_{\text{R}}(t) + \boldsymbol{S}_{\text{R}}U(t), \tag{13b}$$

where X_{R} is the new state vector of low dimension n ($n \ll N$), relatively to the diagonal matrix $\boldsymbol{F}_{\text{R}}$ which contains the n dominant eigenmodes of the system. $\hat{Y}(t)$ is the corresponding output vector such as $\hat{Y}(t) \approx Y(t)$ for any $U(t)$. $\boldsymbol{G}_{\text{R}}$, $\boldsymbol{S}_{\text{R}}$ and $\boldsymbol{H}_{\text{R}}$ are the equivalent new reduced matrices. In our case, the contribution of $\boldsymbol{S}_{\text{R}}U(t)$ in $\hat{Y}(t)$ is the same as the contribution of $\boldsymbol{S}U(t)$ in $Y(t)$ of Eq. (10b), so $\boldsymbol{S}_{\text{R}} = \boldsymbol{S}$. This enables us to keep any stationary states between DM and RM: the reduction will take place only on the dynamical part.

The reduction operation here consists in the fact that the differential system represented by Eq. (13a): (i) is low ordered; and (ii) is much easier to compute than Eq. (3a) because the variables are uncoupled ($\boldsymbol{F}_{\text{R}}$ is diagonal). The principle of model reduction is shown in Fig. 1. This RM will be then more convenient for the inversion.

In the following paragraphs, in order to lighten the notations, RM will be noted in the same way as Eqs. (10a) and (10b):

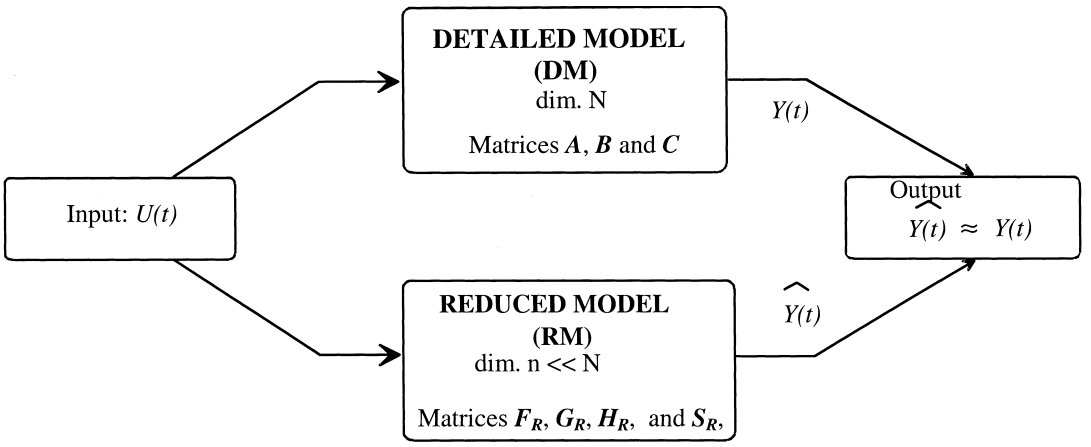

Fig. 1. The principle of model reduction for a state representation.

$$\dot{X}(t) = \boldsymbol{F}X(t) + \boldsymbol{G}\dot{U}(t), \tag{14a}$$

$$Y(t) = \boldsymbol{H}X(t) + \boldsymbol{S}U(t). \tag{14b}$$

Note that several inputs are included in $U(t)$. In order to set up the RM Eqs. (14a) and (14b), several elementary reduced models, built on each component of U are used.

2.3. Elementary reduced model (ERM)

As the assumption of linearity is made, the superposition principle will be applied. In fact, RM is constructed with as many ERMs as components of U: each component $U_i(t)$ is associated to an ERM. Let $u(t) = U_i(t)$ $(1 \leqslant i \leqslant p)$ be the current component of U. Each ERM has a similar structure as Eqs. (14a) and (14b) and can be written as:

$$\dot{x} = \boldsymbol{f}x(t) + g\dot{u}(t), \tag{15a}$$

$$y(t) = \boldsymbol{h}x(t) + su(t), \tag{15b}$$

where x (dim. m) is a new state vector relatively to u, with its eigenvalues included in $\boldsymbol{f}$. The output vector y represents the contribution of the $u(t)$ effect in the final output vector $Y(t)$ of Eq. (14b).

The static vector s is simply the ith column of the static matrix $\boldsymbol{S}$, the stationary is the same in DM and RM (cf. Section 2.2). In practice, this vector is obtained by a simulation of a stationary state with DM: if $u = 1$ is applied to DM and if y_{stat} is the corresponding output, Eqs. (15a) and (15b) lead to:

$$s = y_{\text{stat}}.$$

In earlier works [22,23], it has been demonstrated that all the different matrices in Eqs. (15a) and (15b), as well as the order m, can be obtained with an identification procedure that consists in the minimization of a quadratic criterion relative to the difference between the simulated outputs of DM and the analytical outputs of ERM when a unit step is applied on each model. For a given order m, this criterion J_{red} is written as

$$J_{\text{red}}(\boldsymbol{f}, \boldsymbol{g}, h) = \sum_{i=1}^{q}\sum_{k=1}^{\text{nt}}[y_{ik}(\text{DM}) - y_{ik}(\text{ERM})]^2 \tag{16}$$

where nt is the number of time steps contained in the q outputs. Conjugated gradients and least square method are used for this optimization problem. The method is iterative with the order m which is increased until that $J_{\text{red}}(m+1) \approx J_{\text{red}}(m)$ and the corresponding optimal values of $\boldsymbol{f}$, $\boldsymbol{h}$, and g are then kept for ERM.

2.4. RM reconstitution and its time discretization

When all the p ERMs are identified, with the superposition principle, the matrices of the complete RM (Eqs. (14a) and (14b)) then have the following form:

$$X = \begin{bmatrix} x_1 \\ \cdots \\ \boxed{\text{x}} \\ \cdots \\ x_p \end{bmatrix} \quad F = \begin{bmatrix} f_1 & & & & \\ & \cdots & & 0 & \\ & & \boxed{\text{f}} & & \\ & 0 & & \cdots & \\ & & & & f_p \end{bmatrix}$$

$$G = \begin{bmatrix} g_1 & & & & \\ & \cdots & & 0 & \\ & & \boxed{\text{g}} & & \\ & 0 & & \cdots & \\ & & & & g_p \end{bmatrix} \quad H = [h_1 \quad \cdots \boxed{\text{h}} \quad \cdots h_p]'$$

$$S = [s_1 \quad \cdots \boxed{\text{s}} \quad \cdots s_p] \tag{17}$$

where x, $\boldsymbol{f}$, g, $\boldsymbol{h}$ and s are the current elements coming from Eqs. (15a) and (15b). The RM order will then be $n = \sum m$, m being the current dimension of ERM relatively to u.

The main advantage of this representation is that each input acts with its own dynamics in relation to the output vector. Consequently, the inputs have uncoupled influences. This property will allow the inversion procedure.

By assuming that $U(t) = U(k+1)$ constant between $k\Delta t$ and $(k+1)\Delta t$, the time discretization of Eq. (14a) gives (see Appendix A)

$$X(k+1) = \exp(\boldsymbol{F}\Delta t)\{X(k) + \boldsymbol{G}[U(k+1) - U(k)]\}. \tag{18}$$

It ensues a linear relation between the output vector $Y(k+1)$ and the input vector $U(k+1)$

$$Y(k+1) = [\boldsymbol{H}\ \exp(\boldsymbol{F}\Delta t)\boldsymbol{G} + \boldsymbol{S}]U(k+1) + \boldsymbol{H}\ \exp(\boldsymbol{F}\Delta t)[X(k) - \boldsymbol{G}U(k)]. \tag{19}$$

Eq. (19) enables then the computation of the output vector Y for each time step, when $U(k)$ is known (forward problem).

Remark. Let us underline the parallel with Duhamel's theorem [4] that needs the responses of unit step solicitations on the boundary in order to calculate a convolution integral. The main differences are here: (i) the whole temperature field is not calculated here, (ii) the past of the system at time t is summarized in a low-dimensional state vector $X(t)$ and the convolution is then avoided as it is shown in Eq. (19).

3. Inverse algorithm

3.1. Function specification method

In order to invert, RM will be used. The procedure is sequential: determination of the input vectors: $U(1), U(2), \ldots, U(k), U(k+1), \ldots, U(k_{\text{end}})$ from the output vectors: $Y_m(1), Y_m(2), \ldots, Y_m(k), Y_m(k+1), \ldots, Y_m(k_{\text{end}})$ that represent the measurements. Knowing the input vector $U(k)$ at the time step k, the aim is to identify the vector $U(k+1)$ from the temperatures included in $Y_m(k+1)$. In order to take into account the lagging and damping effects of the diffusion effect, it can be necessary to obtain information using future time steps (FTS) [2]. A function specification is traditionally introduced: a temporary assumption is made on the additional unknowns: $U(k+1+1), \ldots, U(k+1+\text{nf})$, where nf is the number of FTS. We choose here

$$U(k+1+i) = U(k+1) = \text{constant} \quad \text{for } 1 \leqslant i \leqslant \text{nf}. \tag{20}$$

According to Eq. (19), the relations between the output and input vectors at $k+1$ for all FTS (i being the current one) can be written as:

$$\begin{aligned} &Y(k+1) = \boldsymbol{C}_0 U(k+1) + b_0, \\ &\ldots\ldots\ldots\ldots\ldots\ldots\ldots \\ &Y(k+1+i) = \boldsymbol{C}_i U(k+1) + b_i \quad \text{for } 0 \leqslant i \leqslant \text{nf} \end{aligned} \tag{21}$$

with

$$\boldsymbol{C}_i = \boldsymbol{H}\ \exp[(i+1)\boldsymbol{F}\Delta t]\boldsymbol{G} + \boldsymbol{S} \quad \text{for } 0 \leqslant i \leqslant \text{nf} \tag{22}$$

and

$$b_i = \boldsymbol{H}\ \exp[(i+1)\boldsymbol{F}\Delta t][X(k) - \boldsymbol{G}U(k)] \tag{23}$$

The $(\text{nf}+1)$ Eq. (21) can be written under a macro vector form

$$\mathbf{Y} = \mathbf{C}U(k+1) + \mathbf{b} \tag{24}$$

with

$$\mathbf{C} = \begin{bmatrix} \boldsymbol{C}_0 \\ \boldsymbol{C}_1 \\ \cdots \\ \boldsymbol{C}_i \\ \cdots \\ \boldsymbol{C}_{nf} \end{bmatrix} \quad \mathbf{b} = \begin{bmatrix} b_0 \\ b_1 \\ \cdots \\ b_1 \\ \cdots \\ b_{nf} \end{bmatrix} \quad \mathbf{Y} = \begin{bmatrix} Y(k+1) \\ Y(k+1+1) \\ \cdots \\ Y(K+1+i) \\ \cdots \\ Y(K+1+\text{nf}) \end{bmatrix}. \tag{25}$$

Eq. (24) is then a system of $(\text{nf}+1) \times q$ equations which are the components of $\mathbf{Y}$, with p unknowns which are the components of $U(k+1)$. Note that there are more temperatures than unknowns because: (i) there are at least as many sensors as unknowns ($q \geqslant p$); and (ii) future temperatures are used. In order to use now the vector of measurements $\mathbf{Y}_m$, the minimization of a quadratic norm of $\mathbf{Y} - \mathbf{Y}_\mathbf{m}$ (least square method) leads to the resolution of the squared system:

$$\mathbf{C}^{\mathrm{T}}\mathbf{C}\hat{U}(k+1) = \mathbf{C}^{\mathrm{T}}(\mathbf{Y}_m - \mathbf{b}) \tag{26}$$

whose solution is:

$$\hat{U}(k+1) = (\mathbf{C}^{\mathrm{T}}\mathbf{C})^{-1}\mathbf{C}^{\mathrm{T}}(\mathbf{Y}_m - \mathbf{b}). \tag{27}$$

Remark. (i) The ill-posed feature of the inverse problem appears in the difficulty of solving Eq. (26), i.e., the condition number of matrix $\mathbf{C}^{\mathrm{T}}\mathbf{C}$ is large. The condition number can be taken as the ratio of the greatest eigenvalue of $\mathbf{C}^{\mathrm{T}}\mathbf{C}$ to the smallest one. Nearer this number is close to one, better is the conditioning.

(ii) The addition of future time steps is a regularization procedure which acts directly on the matrix to invert: it decreases the condition number of matrix $\mathbf{C}^{\mathrm{T}}\mathbf{C}$.

(iii) The past of the system is represented in vector $\mathbf{b}$ which is calculated with the previous input vectors

$\hat{U}(1), \hat{U}(2), \ldots, \hat{U}(k)$. Compared to a classical transfer function method, this approach allows the non-handling of the time discretization of the transfer function.

(iv) It is also possible to use Tikhonov's penalization [4,5] to regularize Eq. (26). Such an approach has not been necessary here for the inversion with RM.

3.2. Sensitivity coefficients

In order to analyze the possibility to invert with RM, we present here a sensitivity approach based on two concepts: the static and the dynamic sensitivity matrices. Let us underline that our RM is particularly well adapted to point out the sensitivities. First, consider the static matrix $\boldsymbol{S}$ written in Eqs. (14a) and (14b). This one can be considered as a sensitivity matrix, in fact, in stationary cases, each element S_{ij} can be written as:

$$S_{i,j} = \frac{\Delta Y_i}{\Delta U_j} \quad \text{for } \Delta U_j \neq 0 \text{ and } \Delta U_k = 0 \quad \text{for } k \neq j. \tag{28}$$

If two columns of this matrix are quasi proportional, the sensitivities are too correlated and the static inversion is not possible. In order to invert in the transient case, it is also necessary to evaluate the sensitivities in a dynamic way. This is the reason why we introduce the dynamic sensitivity matrix, which is linked to the time step. This matrix $\boldsymbol{S}_{\mathrm{d}}(\Delta\tau)$ is defined from Eq. (22) with $i = 0$:

$$\boldsymbol{S}_{\mathrm{d}}(\Delta t) = \boldsymbol{C}_0 = \boldsymbol{H}\ \exp[\boldsymbol{F}\Delta t]\boldsymbol{G} + \boldsymbol{S} \tag{29}$$

and represents the evolution of the static matrix after one time step. When Δt tends toward zero, $\boldsymbol{S}_{\mathrm{d}}$ tends toward the null matrix, this formulation shows that $\boldsymbol{S}$ is an upper limit for $\boldsymbol{S}_{\mathrm{d}}$: the static sensitivities will always be greater than the dynamic ones. So it can be seen that if Δt is too low for the system, $\boldsymbol{S}_{\mathrm{d}}$ is near 0: the dynamic sensitivities are too weak and the inversion is delicate. When Δt becomes greater, matrix $\boldsymbol{S}$ contribution becomes heavier and the sensitivity coefficients are better. So, in order to strengthen these coefficients, two possibilities can be envisaged: (i) the increase of Δt, (ii) the use of nf future time steps through matrices defined by Eq. (22). Of course, when Δt or nf increases, the condition number of matrix $\mathbf{C}^{\mathrm{T}}\mathbf{C}$ of Eq. (22) is modified.

4. Applications

4.1. Description of the 2D system and aim of the study

The system under investigation is a square slab ABCD ($AB = 0.1$ m) composed of stainless steel ($k = 16$ $\mathrm{W\,m^{-1}\,°C^{-1}}$, $C_{\mathrm{P}} = 510$ $\mathrm{J\,kg^{-1}\,°C^{-1}}$, $\rho = 7900$ $\mathrm{kg\,m^{-3}}$). Fig. 2 shows the geometry with its boundary conditions: two heat flux densities $\varphi_1(t)$ on AD, $\varphi_2(t)$ on AB and two convective boundary conditions relative to a fluid temperature $T_{\mathrm{f}} = 0$°C ($h = 100$ $\mathrm{W\,m^{-2}\,°C^{-1}}$on BC and $h = 10$ $\mathrm{W\,m^{-2}\,°C^{-1}}$on CD).

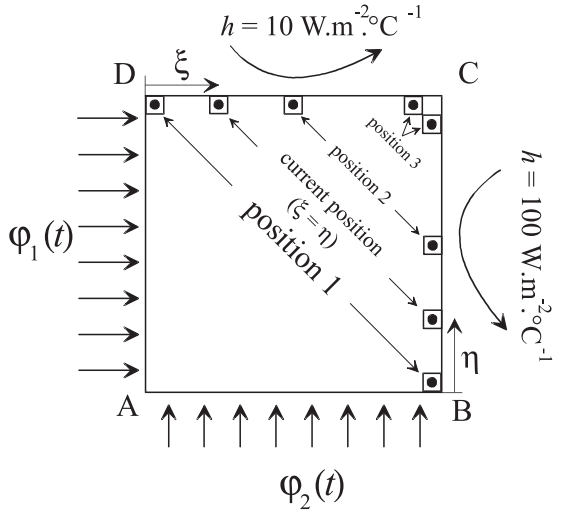

Fig. 2. The 2D diffusive system with the three studied positions of sensors and the current one.

At first, in order to obtain a detailed model under the form (Eqs. (3a) and (3b)), the domain is modeled with a classical control volume method with a regular mesh (11×11). The temperatures on the 121 nodes represent the temperature field whose values constitute the components of vector T (Eqs. (3a) and (3b)). The two heat flux densities $\varphi_1(t)$ and $\varphi_2(t)$ are set in the output vector $U(t)$ ($p = 2$). In the output vector, $Y(t)$ are set the node temperatures on two points ($q = 2$) among the 121. These two points represent two sensors: one located along the side BC and the other on side CD.

Now the stages are the following: first, we present a study of sensitivities based on an RM built on the two sensors in the current position (Fig. 2). Then, an example of reduction is shown. Finally, for the inversion, three different positions of the two sensors are studied in an increasing difficulty with their own RM: position 1, i.e., close to the thermal solicitations, position 2 in the middle of the sides, and position 3, the farthest away from the solicitations.

4.2. Sensitivity study

4.2.1. Static sensitivities

According to the study presented in Section 3.2, we present the static sensitivities when the sensors (Fig. 2) are moved simultaneously ($\xi = \eta$) respectively on CD (Fig. 3) and on BC (Fig. 4). It can be noted that:

- Globally, both sensors are sensitive to both inputs.
- The level of sensitivity gives interesting information relative to the level of the heat flux density that can

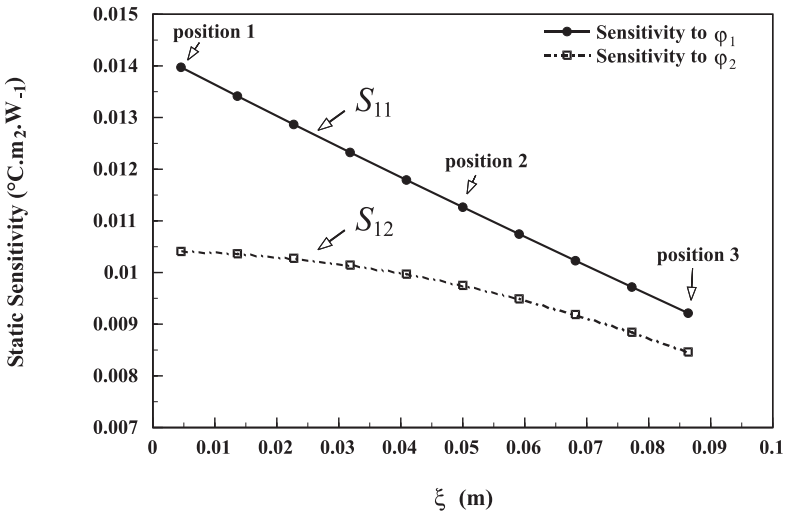

Fig. 3. Static sensitivities vs. ξ (along DC).

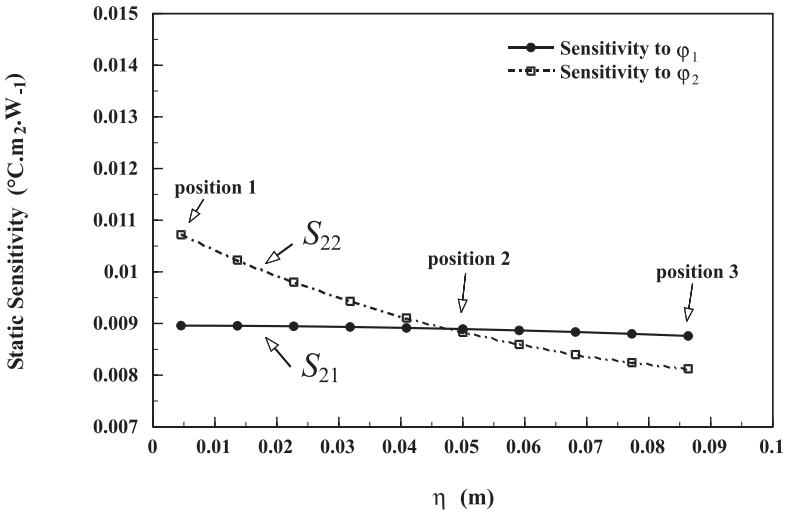

Fig. 4. Static sensitivities vs. η (along BC).

be identified. For example, if the sensitivity is 0.01 $m^2\,W^{-1}\,°C$, with a sensor which has a precision under 1°C, an identification less than 100 $W\,m^{-2}$ will be impossible.

- The first sensor (on CD, Fig. 3) is always more sensitive to φ_1 than to φ_2 ($S_{11} > S_{12}$).
- Even in position 1 (the most uncoupled and the easiest position), S_{12} is as important as S_{22}, and S_{12} remains higher than S_{22} when the sensors move away from position 1. Such an analysis is not possible when considering only the system intuitively with Fig. 2. This is due to the thermal asymmetry coming from the different boundary conditions along the sides DC ($h = 10$ $W\,m^{-2}\,°C^{-1}$) and BC ($h = 100$ $W\,m^{-2}\,°C^{-1}$).
- For the same reason, at the middle of BC (position 2), S_{22} becomes lower than S_{21} when η increases (Fig. 4). Taking into account, the geometry of the system and its boundary conditions, we see then, that the static sensitivities to φ_1 dominate the φ_2 ones.

4.2.2. Dynamic sensitivity

Now let us analyze the dynamic sensitivities given by Eq. (23). Firstly, let us consider the sensitivities when no FTS are used (nf = 0). They are represented in Fig. 5 for the first sensor on CD (the 2nd sensor is not presented as

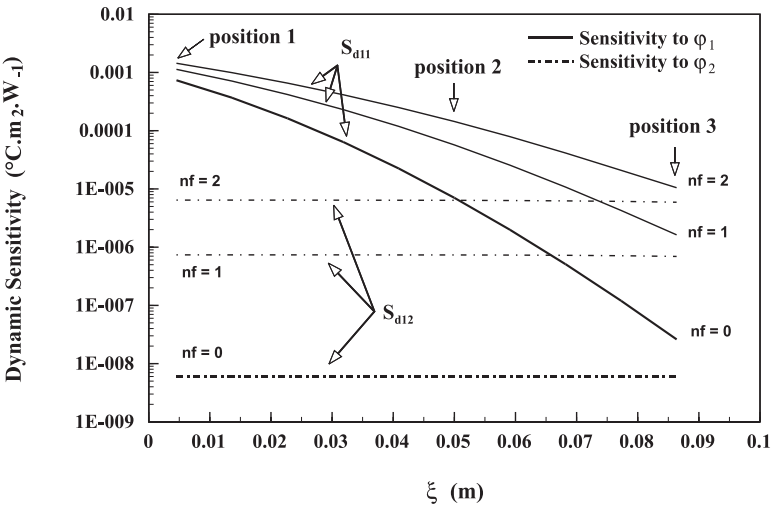

Fig. 5. Dynamic sensitivities vs. ξ (along DC) for nf = 0, 1 and 2 with $\Delta t = 50$ s.

the sensitivities are quite similar). Of course, as it has been demonstrated in Section 3, these sensitivities are lower than the static ones and depend on the time step, which is used. In Fig. 5, we can see the effect of adding FTS: it appears clearly that the dynamic sensitivities significantly increase when FTS are used. This effect is especially visible when nf increases from 0 to 1. The dynamic sensitivity of the points far from the excitations (position 3) is multiplied by a factor greater than 100. On the contrary, for the sensors close to the excitations ($\boldsymbol{S}_{d11}$ on the left), the addition of FTS has almost no influence.

4.2.3. Decoupling

In order to invert, of course the sensitivities must be sufficient, but as there are two unknowns, the sensitivities must not be correlated. The correlation can be appreciated with the determinants:

$$\det(\boldsymbol{S}) = \begin{vmatrix} S_{11} & S_{12} \\ S_{21} & S_{22} \end{vmatrix} \quad \text{and} \quad \det(\boldsymbol{S}_d) = \begin{vmatrix} S_{d11} & S_{d12} \\ S_{d21} & S_{d22} \end{vmatrix},$$

respectively for the static and dynamic sensitivities.

These values must be as great as possible. They are given in Table 1 for the three positions. They decrease with the distance from the heat flux densities. In this case, the optimum location of the sensors is of course position 1 because the dynamic sensitivities and the determinants are the greatest.

In a general way, whatever the sensitivities may be, it is essential to study the decoupling between the sensors. Of course, the most favorable case is when a sensor has a large sensitivity to one excitation and a small one to the other excitation and vice versa. It is then foreseeable that the inversion results will become less satisfactory when the sensors approach point *C*.

4.3. Construction and validation of RM

From the current position, an RM is built according to Section 2. As an example, we show here the results corresponding to position 2. On each input, ERM is identified. As an illustration, the dominant eigenvalues expressed as time constants τ_i and the quadratic criterion J_{red} (Eq. (16)) for both ERMs at different orders are shown in Table 2.

Comments:

- Of course, the criterion J_{red} decreases when the order m increases (strongly between $m = 2$ and 3): the lower this criterion, the better the ERM.
- The main time constants are found for $m = 3$ in both ERMs ($\tau_i = 4288$ s), and the others, a little different, allow the simulation of faster dynamics.
- Even if two identical (or quasi) time constants appear in both ERMs, their influences are nevertheless separated through the entire reduced model given by Eqs. (14a), (14b) and (17). For example, it can be

Table 1
Determinants of static and dynamic matrices according to the position of both sensors

Position	1	2	3
$\det(\boldsymbol{S})$	5.65×10^{-5}	1.27×10^{-5}	7.28×10^{-7}
$\det(\boldsymbol{S}_d)$	5.25×10^{-7}	7.25×10^{-12}	3.38×10^{-15}

Table 2
Time constants and quadratic criterion for each ERM in position 2

		ERM order		
		2	3	4
Input 1	Time constants τ_i (s)	4266	4288	4288
$u_1 = \varphi_1$		267	227	228
			83	76
				9
	J_{red} (°C^2)	0.128×10^{-6}	0.589×10^{-9}	0.161×10^{-9}
Input 2	Time constants τ_i (s)	4263	4288	4288
$u_2 = \varphi_2$		296	240	242
			82	74
				8
	J_{red} (°C^2)	0.114×10^{-6}	0.556×10^{9}	0.191×10^{9}

seen in Table 2 for $m = 4$ that, on each input, the main time constant (4288 s) has been identified: consequently this value appear twice (in matrices $\boldsymbol{f}_1$ and in $\boldsymbol{f}_2$) but is treated differently through matrices $\boldsymbol{h}_1$ and in $\boldsymbol{h}_2$ and vectors g_1 and g_2 of Eq. (17). This last formulation is then quite different of the similar one (Eq. (11)) corresponding to the diagonalization of the state-space matrix of DM, where the eigenvalues are usually very different.

When both ERMs are identified, the final RM is built (Eq. (17)). Before using it for the inversion, we propose here a validation: a comparison between RM and DM temperature evolutions in position 2 for a same input set (the inputs that will be used after for inversion and that are represented in Fig. 8). These direct simulations are made with a time step $\Delta t = 50$ s, so we choose $m = 3$ for each ERM: in fact, time constants smaller than 10 s are not representative enough for such Δt (cf. Table 2). For example, Fig. 6 shows two responses (middle of BC) which seem equivalent: the temperature difference must be multiplied by 100 to be visible on the graph. Therefore, RM gives very accurate responses and can be used for inversion.

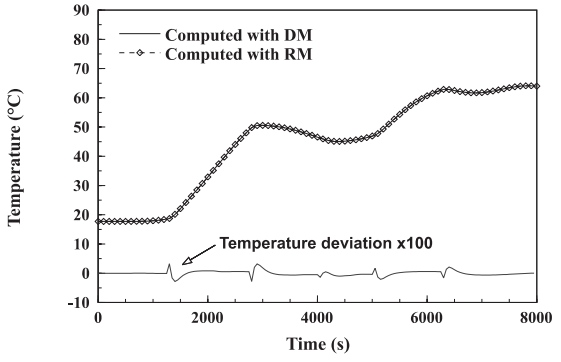

Fig. 6. Comparison of DM (order 121) and RM (order 6) temperature evolutions for the same inputs. Position 2. $\Delta t = 50$ s.

4.4. Inversion results

In this part, positions 1, 2 and 3 will be used for the inversion. Each of these positions is represented by RM with Eqs. (14a) and (14b). The temperature evolutions of the sensors are computed with DM (Eqs. (3a) and (3b)) and RM is used for the inverse procedure. Knowing the true applied heat flux densities, the quality of the inversion results will be given by:

$$\sigma_U = \left[\frac{1}{(\mathrm{nt} - 1 - \mathrm{nf}) \times p} \times \sum_{i=1}^{p} \sum_{k=1}^{(\mathrm{nt}-1-\mathrm{nf})} \left(U_i(k) - \hat{U}_i(K) \right)^2 \right]^{1/2}, \tag{30}$$

where U is the exact input vector, $\hat{U}$ the identified one and nt is the number of time steps that are used. Similarly, a measure of the difference between the original temperatures included in Y (the simulated data with DM) and the computed ones included in $\hat{Y}$ (calculated with the identified inputs) can be written:

$$\sigma_Y = \left[\frac{1}{(\mathrm{nt} - 1 - \mathrm{nf}) \times q} \times \sum_{i=1}^{q} \sum_{k=1}^{(\mathrm{nt}-1-\mathrm{nf})} \left(Y_i(k) - \hat{Y}_i(k) \right)^2 \right]^{1/2}. \tag{31}$$

It gives an estimated standard deviation of the temperatures. Of course, in real applications, σ_Y is the only value that can be reached. σ_U is given here as supplementary information.

Furthermore, to simulate measurement errors, each temperature included in Y is altered with an additive Gaussian error. A simulated noisy data T^* can then be expressed as

$$T^* = T_{\mathrm{exact}} + \omega\sigma, \tag{32}$$

where σ is the standard deviation of the measurement errors which are supposed to be the same for all

measurements and ω is a random Gaussian variable such as $-2.576 < \omega < 2.576$ that corresponds to the 99% confidence bounds for the temperature measurement. For all test cases analyzed here, we consider $\sigma = 0°C$ (errorless measurements), $\sigma = 0.1°C$ and $\sigma = 0.2°C$ (noisy data).

As an example of results, let us consider position 2. From the temperatures altered with an additive noise ($\sigma = 0.1°C$), represented in Fig. 7, we present the results of the inversion in Fig. 8 as well as the exact values. The

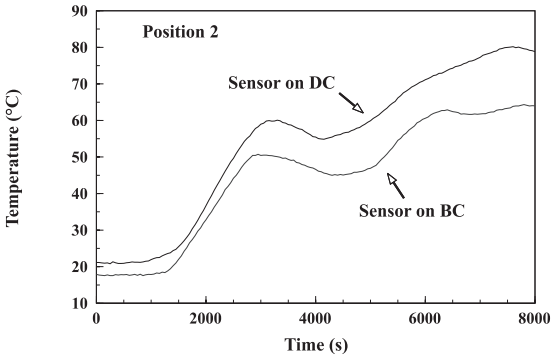

Fig. 7. Temperature evolutions in position 2 ($\sigma = 0.1°C$). $\Delta t = 50$ s.

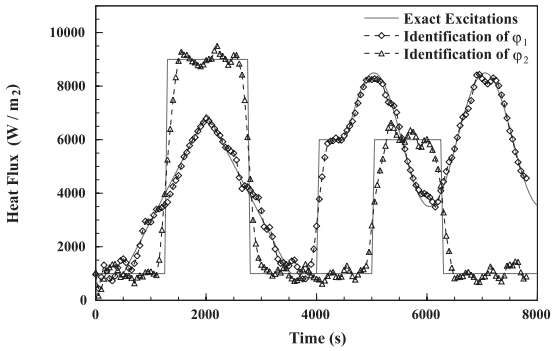

Fig. 8. Identification of φ_1 and φ_2 from two sensors in position 2 with $\sigma = 0.1°C$ and nf = 4.

results are quite satisfying ($\sigma_Y = 0.104°C$ and $\sigma_U = 611\ W\,m^{-2}$). Thanks to RM composed of two ERMs, the contribution of each input to the sensor temperature could be restored, although the solicitations vary in a very different manner (Fig. 8). Note that the influence of these evolutions is smoothed when considering the evolutions of temperature (Fig. 7).

All the inversion results are summarized in Table 3 for the three different positions.

Comments:

(a) *Errorless measurements*: When no measurement error is added to the simulated temperatures, for position 1, no future time step is needed (nf = 0) and σ_Y is very low (1.8×10^{-14} °C). However, the value of σ_U (408 $W\,m^{-2}$) is penalized when the solicitations vary suddenly vs. time. It is nevertheless acceptable compared to the level of these solicitations. It represents the best value that can be obtained.

For positions 2 and 3, σ_Y and σ_U increase, as well as the number of FTS. Nevertheless, the identifications can be considered as good. Note that the optimum number of FTS is obtained when σ_Y is minimum.

(b) *Noisy data*: Now, to check the efficiency and accuracy of the algorithm, the effect of measurement errors is studied. When there are measurement errors, nf has to be increased until $\sigma_Y \approx \sigma$. This corresponds to a regularization procedure. Of course, the problem becomes more difficult. Table 3 shows that the estimations of φ_1 and φ_2 become less good when the measurement error increases. For position 3 (where the lagging and damping effects are very important) and with a noise level equal to $\sigma = 0.2°C$, the identification of φ_1 and φ_2 is not physically acceptable.

(c) *Effect of the number of future time steps on the condition number*: As an example, for position 2, the condition number (CN) of matrix $\mathbf{C}^T\mathbf{C}$ (Eq. (26)) is given in Table 4.

For errorless measurements, it can be seen how CN decreases abruptly between nf = 0 and nf = 1. Moreover, it corresponds to the best CN compared to the other cases, and the inversion is correct.

When $\sigma = 0.1°C$, it has been necessary to use nf = 4 to invert, i.e., to obtain worthy results. Nevertheless, the

Table 3
Effect of the standard deviation for the three positions

σ (°C)		0	0.1	0.2
Position 1	σ_Y	1.8×10^{14}	1.9×10^{14}	2.0×10^{14}
	σ_U	408	408	430
	nf	0	0	0
Position 2	σ_Y	2.05×10^{3}	0.104	0.244
	σ_U	453	611	725
	nf	1	4	6
Position 3	σ_Y	1.10×10^{3}	0.112	
	σ_U	500	1400	
	nf	2	7	

Table 4
Influence of the number of FTS nf on the condition number (CN)

nf	0	1	2	3	4
CN	29.7	1.23	1.24	1.40	1.67

correspondent CN is acceptable (1.67) and the value of σ_Y (0.104°C) is just over the noise standard deviation ($\sigma = 0.1$°C, cf. Table 3). This is in accordance with classical studies on inverse results from noisy data [4,5] where the estimated standard deviation of the temperatures corresponds to the noise.

4.5. A 3D application

We propose here a 3D application by simply adding a third dimension to the previous system. A cube of stainless steel is then studied with a third heat flux density φ_3. A third boundary condition, with $h = 50$ W m^{-2} °C^{-1} relatively to 0°C, is assumed on the opposite face. The corresponding DM, established with control volumes (order $1331 = 11 \times 11 \times 11$), is computed with Eqs. (3a) and (3b). In the output vector are set three temperatures that simulate three sensors set in the middle of opposite faces (analogy of position 2 in the 2D case). As the input vector is made with 3 heat flux densities (φ_1, φ_2, φ_3), three ERM are identified and the corresponding RM is here of order $m = 9$ (order 3 for each ERM).

The three simulated measurements to invert are presented in Fig. 9. From these values and with an added noise ($\sigma = 0.1$°C), we present the results of the inversion with the original inputs in Figs. 10–12. The use of nf = 4 has been necessary here. When seeing the three smooth temperature evolutions (Fig. 9), the quality of these results must be underlined. Moreover, it has been computed with a model of order nine instead of the original one of order 1331.

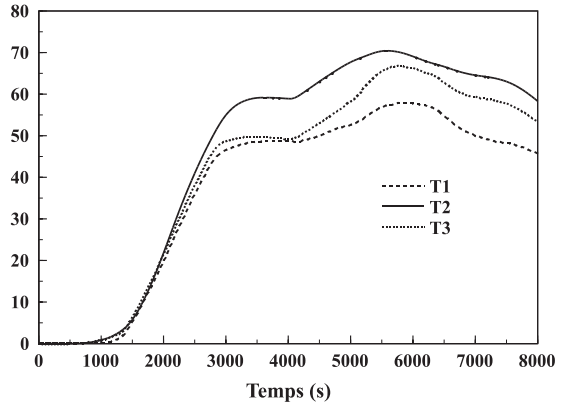

Fig. 9. Simulated measurements.

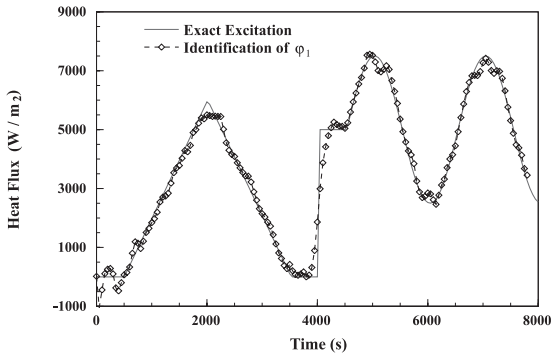

Fig. 10. Identification of φ_1 with $\sigma = 0.1$°C and nf = 4. $\Delta t = 50$ s.

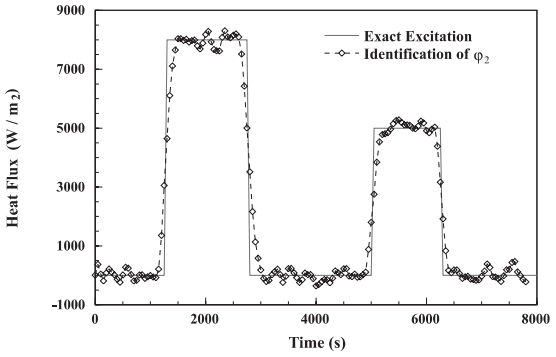

Fig. 11. Identification of φ_2 with $\sigma = 0.1$°C and nf = 4. $\Delta t = 50$ s.

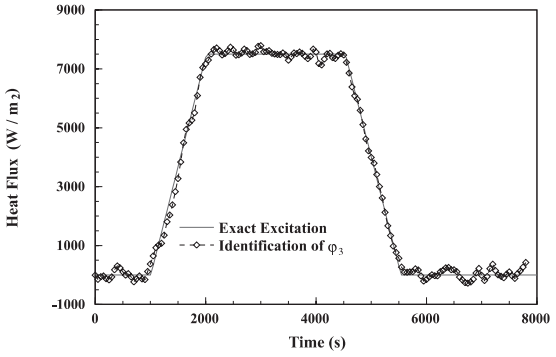

Fig. 12. Identification of φ_3 with $\sigma = 0.1$°C and nf = 4. $\Delta t = 50$ s.

4.6. Computer time

Besides the possibility to easily invert 3D IHCPs, an important advantage of RM consists in the quickness of the computations. In fact, on the one hand, the CPU time is low due to RM dimension. On the other hand, the modal representation decreases the computational

time because of the uncoupling of the state variables: the reduced matrix $\boldsymbol{F}$ of Eq. (14a) is diagonal, which reduces the number of operations. For instance, when solving the 3-D IHCP, the CPU time was about 3×10^{-3} s per time step (on a work station): this advantage can be used efficiently, particularly with the aim of controlling a process in real time. Of course, the main computation effort has been made before, for the building of the different ERMs [22,23], but this is made once and for all.

5. Conclusion

In this paper, the use of a reduced model for the solution of IHCP is introduced. The method includes the regularization with the function specification technique and gives accurate results. In fact, RM underlines directly and separately the contribution of each thermal input to the observed outputs. A deconvolution of the temperatures is then possible. On a 2D example, whose reduction ratio was 121 (DM)/6 (RM), the different positions of the sensors are analyzed by the study of the static and dynamic sensitivities: these last ones show the influence of the time step and the number of future time steps. Good results are obtained as well as in a 3D application whose reduction ratio is much more interesting with 1331 (DM)/9 (RM).

Let us point out that the proposed method is particularly robust in multidimensional IHCPs: RM does not "see" the 2D or 3D aspect of the phenomena. In fact, the resolution is made only on the sensor locations: RM links the inputs and outputs through the reduced modal formulation. Moreover, the method is computationally efficient: an interesting application of IHCP using RM is the possibility to include it in a control-command process in real time.

At present, the continuation of this work consists in its application to experimental situations with real measurements.

Appendix A

It is shown that the analytical solution of the state equation:

$$\dot{X}(t) = \boldsymbol{F}X(t) + \boldsymbol{G}\dot{U}(t) \tag{A.1}$$

is given by:

$$X(t) = \mathrm{e}^{\boldsymbol{F}(t-t_0)}X(t_0) + \int_{t_0}^{t} \mathrm{e}^{\boldsymbol{F}(t-\tau)}\boldsymbol{G}\dot{U}(\tau)\,\mathrm{d}\tau.$$

We use this analytical solution between $k \times \Delta t$ and $(k+1) \times \Delta t$:

$$X(k+1) = \mathrm{e}^{\mathbf{F}\Delta t}X(k) + \int_{k\Delta t}^{(k+1)\Delta t} \mathrm{e}^{\mathbf{F}[(k+1)\Delta t-\tau]}\mathbf{G}\dot{U}(\tau)\,\mathrm{d}\tau$$

$$X(k+1) = \mathrm{e}^{\mathbf{F}\Delta t}X(k) + \mathrm{e}^{\mathbf{F}(k+1)\Delta t} \int_{k\Delta t}^{(k+1)\Delta t} \mathrm{e}^{-\mathbf{F}\tau}\mathbf{G}\dot{U}(\tau)\,\mathrm{d}\tau$$

By integrating the second term by parts

$$\begin{aligned} X(k+1) &= \mathrm{e}^{\mathbf{F}\Delta t}X(k) + \mathrm{e}^{\mathbf{F}(k+1)\Delta t}\left[\left[\mathrm{e}^{-\mathbf{F}\tau}\mathbf{G}U(\tau)\right]_{k\Delta t}^{(k+1)\Delta t} + \mathbf{F}\int_{k\Delta t}^{(k+1)\Delta t} \mathrm{e}^{-\mathbf{F}\tau}\mathbf{G}U(\tau)\,\mathrm{d}\tau\right] \\ &= \mathrm{e}^{\mathbf{F}\Delta t}X(k) + \mathrm{e}^{\mathbf{F}(k+1)\Delta t}\left[\left[\mathrm{e}^{-\mathbf{F}(k+1)\Delta t}\mathbf{G}U(k+1) - \mathrm{e}^{-\mathbf{F}k\Delta t}\mathbf{G}U(k)\right] + \mathbf{F}\int_{k\Delta t}^{(k+1)\Delta t} \mathrm{e}^{-\mathbf{F}\tau}\mathbf{G}U(\tau)\,\mathrm{d}\tau\right]. \end{aligned}$$

By writing that $U(\tau) = U(k+1)$ between time steps $k \times \Delta t$ and $(k+1) \times \Delta t$, we obtain

$$\begin{aligned} X(k+1) &= \mathrm{e}^{F\Delta t}X(k) + \mathrm{e}^{F(k+1)\Delta t} \\ &\quad \left[\left[\mathrm{e}^{-F(k+1)\Delta t}\mathbf{G}U(k+1) - \mathrm{e}^{-Fk\Delta t}\mathbf{G}U(k)\right] + FGU(k+1)\int_{k\Delta t}^{(k+1)\Delta t} \mathrm{e}^{-Fv}\,\mathrm{d}v\right] \\ &= \mathrm{e}^{F\Delta t}X(k) + \mathrm{e}^{F(k+1)\Delta t}\left[\left[\mathrm{e}^{-F(k+1)\Delta t}\mathbf{G}U(K+1) - \mathrm{e}^{-Fk\Delta t}\mathbf{G}U(k)\right] - \mathbf{G}U(k+1)\left[\mathrm{e}^{-F\tau}\right]_{k\Delta t}^{(K+1)\Delta t}\right] \\ &= \mathrm{e}^{F\Delta t}X(k) + \mathrm{e}^{F(k+1)\Delta t}\left[\left[\mathrm{e}^{-F(k+1)\Delta t}\mathbf{G}U(k+1) - \mathrm{e}^{-Fk\Delta t}\mathbf{G}U(k)\right] - \mathbf{G}U(k+1)\left[\mathrm{e}^{-F(k+1)\Delta t} - \mathrm{e}^{-Fk\Delta t}\right]\right] \\ &= \mathrm{e}^{F\Delta t}X(k) + \left[\mathbf{G}U(k+1) - \mathrm{e}^{F\Delta t}\mathbf{G}U(k)\right] - \mathbf{G}U(k+1)\left[\mathbf{1} - \mathrm{e}^{F\Delta t}\right]. \end{aligned}$$

Finally, the time discretization of Eq. (A.1) is then

$$X(k+1) = \mathrm{e}^{\mathbf{F}\Delta t}X(k) + \mathrm{e}^{\mathbf{F}\Delta t}\mathbf{G}[U(k+1) - U(k)].$$

References

[1] J.V. Beck, B. Blackwell, A. Haji-Sheikh, Comparison of some inverse heat conduction methods using experimental data, Int. J. Heat Mass Transfer 39 (17) (1996) 3649–3657.

[2] J.V. Beck, B. Blackwell, C.R. St. Clair, Inverse Heat Conduction: Ill-posed Problems, Wiley, New York, 1985, pp. 108–160.

[3] E.P. Scott, J.V. Beck, Analysis of order of the sequential regularization solutions of inverse heat conduction problems, ASME J. Heat Transfer 111 (1989) 218–224.

[4] O.M. Alifanov, Inverse Heat Transfer Problems, Springer, New York, 1994.

[5] O.M. Alifanov, E.A. Artyukhin, S.V. Rumyantsev, Extreme Methods for Solving Ill Posed Problems with Applications to Inverse Heat Transfer, Begell House, New York, 1995, pp. 152–215.

[6] A.M. Osman, K.J. Dowding, J.V. Beck, Numerical solution of the general two-dimensional inverse heat conduction problem, ASME J. Heat Transfer 119 (1997) 38–45.

[7] M. Raynaud, J.V. Beck, Methodology for comparison of inverse heat conduction methods, J. Heat Transfer 110 (1988) 30–37.
[8] C.C. Ji, P.-C. Tuan, H.-Y. Jang, A recursive least-squares algorithm for on-line 1-D inverse heat conduction estimation, Int. J. Heat Mass Transfer 40 (9) (1997) 2081–2096.
[9] F. Scarpa, G. Milano, Kalman smoothing technique applied to the inverse heat conduction problem, Numer. Heat Transfer B 28 (1995) 79–96.
[10] P.-C. Tuan, C.C. Ji, L.-W. Fong, W.-T. Huang, An input estimation approach to on-line two-dimensional inverse heat conduction problems, Numer. Heat Transfer B 29 (1996) 345–363.
[11] C.-H. Huang, C.-W. Chen, A boundary-element-based inverse problem of estimating boundary conditions in an irregular domain with statistical analysis, Numer. Heat Transfer B 33 (1998) 251–268.
[12] C. Le Niliot, The boundary-element method for the time-varying strength estimation of point heat sources: application to a two-dimensional diffusion system, Numer. Heat Transfer B 33 (1998) 301–321.
[13] R. Pasquetti, C. Le Niliot, Boundary element approach for inverse heat conduction problems: application to a bidimensional transient numerical experiment, Numer. Heat Transfer B 20 (1991) 169–189.
[14] Y. Jarny, M.N. Ozisik, J.P. Bardon, A general optimization method using adjoint equation for solving multidimensional inverse heat conduction, Int. J. Heat Mass Transfer 34 (11) (1991) 2911–2919.
[15] D. Petit, V. Debray, C. Le Niliot, R. Pasquetti, Identification of local heat transfer coefficient using a boundary formulation. Comput. Meth. Heat Transfer, 1992, Springer, Milan.
[16] E. Videcoq, D. Petit, H. Sadat, Resolution of inverse heat conduction problem with reduced models, in: Proceedings of 11th International Heat Transfer Conference, Kyongju, Corée, 7, 1998, pp. 89–94.
[17] M. Decoster, A.R. Van Cauwenberghe, A comparative study of different reduction methods (Part 1–2), Journal A 17 (3) (1976) 58–74, 125–135.
[18] P. Bertrand, G. Duc, G. Michailesco, Recent developments in model reduction, RAIRO APII 19 (1985) 131–146.
[19] K. El Khoury, A. Neveu, Analyse modale des systèmes thermiques en présence de transferts non réciproques, Int. J. Heat Mass Transfer 32 (1989) 213–226.
[20] M.T. Ben Jaafar, R. Pasquetti, D. Petit, Model reduction for thermal diffusion: Application of the Eitelberg, Marshall and aggregation methods to a heat transmission tube model, Int. J. Numer. Meth. Eng. 29 (1990) 599–617.
[21] R. Pasquetti, D. Petit, Analyse Modale d'un Processus de Diffusion Thermique: Identification par Thermographie Infra-Rouge, Int. J. Heat Mass Transfer 31 (1988) 487–496.
[22] D. Petit, R. Hachette, D. Veyret, A modal identification method to reduce a high-order model: application to heat conduction modelling, Int. J. Modelling Simulation 17 (3) (1997) 242–250.
[23] E. Videcoq, Problèmes inverses en diffusion thermique instationnaire: résolution par représentation d'état et apport de la réduction de modèle, Thèse de l'Université de Poitiers 19 Novembre 1999.